communications earth & environment

ARTICLE

https://doi.org/10.1038/s43247-022-00404-x OPEN

Growing prevalence of heat over cold extremes with overall milder extremes and multiple successive events

Yuan Zhang[1], Qiangzi Li[1✉], Yong Ge[2,3✉], Xin Du[1] & Hongyan Wang[1]

Temperature extremes with altered characteristics are one of the most threatening impacts of global warming. How their characteristics have changed is uncertain, and varies by region. Here we analyse ERA5 reanalysis data for the period 1980 to 2018 to illuminate the spatio-temporal characteristics of single and multiple successive temperature extreme events at the global scale. We show that in the global average, the magnitude of heat extremes significantly increased while that of cold extremes decreased at a faster rate. As a result, the prevailing climate shifted from a prevalence of cold extremes to one of heat extremes, and the overall magnitude of extremes decreased. Globally, the magnitude of multiple successive temperature extreme events constituted about a quarter of all identified events. These trends were not globally uniform. The most noteworthy trends were observed in the Tropical and Polar zones; the Middle East and North Africa, including the Mediterranean region, were identified as hotspots of climate shifts.

[1] National Engineering Laboratory for Satellite Remote Sensing Applications, Aerospace Information Research Institute, Chinese Academy of Sciences, Beijing, China. [2] State Key Laboratory of Resources and Environmental Information Systems, Institute of Geographic Sciences and Natural Resources Research, Chinese Academy of Sciences, Beijing, China. [3] Southern Marine Science and Engineering Guangdong Laboratory (Zhuhai), Zhuhai, China. ✉email: liqz@aircas.ac.cn; gey@lreis.ac.cn

Globally the air temperature had increased by about 1.09 °C on average in 2011–2020 compared to 1850–1900, and is projected to continue to increase during the 21st century, as confirmed by global Earth system models (ESMs) participating in the Coupled Model Intercomparison Project Phase 6 (CMIP6)[1]. Consequently, characteristics of many extreme climate events have been considerably altered[1–10], which is generally acknowledged as the most threatening effects of global warming[2,11]. Among them, temperature extreme events (TEEs), including heat waves, warm spells, cold waves and cold spells, are directly influenced by global warming[5]. TEEs are associated with notable mortality and morbidity, and also have catastrophic economic and environmental impacts in terms of crop production, workplace productivity, biodiversity, wildfires, air and water quality, cooling/heating costs and public infrastructure[5,10,12–19].

Due to the devastating impacts of TEEs, there have been a rising global interest over various sectors in measuring, characterizing, analysing and understanding them. The frequency and severity of heat extremes increased over most land areas[14,16,18,20–22], while those of cold extremes exhibited decreasing trends[7,10,22,23]. These trends were identified as "virtually certain" in the Intergovernmental Panel on Climate Change (IPCC) Sixth Assessment Report (IPCC AR6)[1]. However, because the global warming pattern and its impacts have not been globally uniform[6,24,25], great spatio-temporal variations can be observed in the patterns and trends of TEE characteristics over different regions[19,26]. Moreover, the increase in heat extremes was found to greatly exceed the decrease in cold extremes in some parts of the world[10,27,28], while the opposite can be observed in other parts[29]. A comprehensive analysis on TEE characteristics at the global scale is therefore necessary to reveal the spatio-temporal variation and uncertainty of TEE dynamics as influenced by climate change, and to support more efficient and effective response and adaptation to climate change.

TEEs have been measured and analysed extensively[26,30–37]. While heat extremes are the most studied events, much less studies focus on cold extremes[23,38,39], and even fewer on both. These studies also mainly deal with summertime heat waves and wintertime cold waves, and adequate analysis still lacks regarding cooler season warm spells and warmer season cold spells[36]. Dearth of multi-perspective insights limits comprehensive and systematic investigation of TEEs. Moreover, most studies treated TEEs as single independent events, neglecting the compounding of multiple TEEs occurring close in time (compound TEEs, see Methods for detailed definition), which is generally associated with increased vulnerability and impacts[40–44]. Dependent on the study areas, sectors, target groups, and application purposes of the studies, TEEs have been investigated using various definitions and metrics[26,36,45,46]. Such discrepancy further hampers the comparison of TEE dynamics over time and across regions.

Therefore, it is still largely unknown at the global scale regarding the spatio-temporal characteristics of TEEs when both heat and cold extremes are considered together, of heat extremes as opposed to cold extremes, and of compound TEEs. Specifically, a few questions remain to be addressed: (1) How did the frequency and severity of heat extremes, cold extremes, and TEEs as a whole change? (2) How did heat and cold extremes change as opposed to each other, and what extremes prevail regionally and globally? (3) What fraction did compound TEEs constitute, and did that change with global warming? And (4) are these trends globally uniform and do they vary by climate zone? In order to find answers to these questions, we designed a comprehensive analytical framework to define and measure single and compound TEEs, and to analyse the spatio-temporal patterns and trends of their annual mean frequency (F), mean event duration (D), mean event intensity (I), and annual cumulative magnitude (M) at grid cell, regional and global scales over the period 1980–2018 (see Methods). We find that globally on average M significantly increased for heat extremes and significantly decreased for cold extremes at a faster rate. As a result, TEEs' M exhibited a significant downward trend, and the world had shifted from a cold-extreme- to a heat-extreme-prevailing climate. Globally compound TEEs constituted about a quarter of all identified TEEs in terms of M, and this proportion exhibited a significant decreasing trend. These trends were associated with great spatial heterogeneity, and noteworthy patterns and trends can be observed in the Tropical and Polar zones identified by the Koppen-Geiger (KG) climate classification system (Supplementary Fig. S1). The findings presented here can improve our understanding of the global and regional patterns and trends of TEEs, and are expected to offer new perspectives on the formulation of more targeted, effective and region-specific strategies of climate change adaptation and greenhouse gas emissions mitigation.

Results and discussion

Patterns and trends of TEEs. Globally, an average number of 2.79 TEEs occurred each year, each TEE lasted for 4.93 days with an intensity of 2.54 °C day^{-1} on average, and all TEEs added up to a cumulative magnitude of 35.72 °C year^{-1} during the period 1980–2018 (Table 1). Both F and M of TEEs exhibited a latitudinal gradient decreasing towards lower latitudes (Fig. 1a and d), where the temperature variability is markedly smaller[47]. A hotspot pattern was exhibited for D, with high values (>5.5 days event^{-1}) concentrated in the Antarctica, Alaska, northeastern and west coast of South America, eastern Africa around Sudan, Tibetan Plateau, and small areas of Southeast Asia (Fig. 1b). Regions with higher I values (3–4 °C day^{-1} event^{-1})) were evident mainly in North America and Russia, and were predominantly located in the Cold zone (Fig. 1c), resulting in the highest regional I value of 3.17 °C day^{-1} event^{-1} (Table 1).

Table 1 TEE metrics and their temporal trends for all identified temperature extreme events (TEEs) in the world and in KG climate zones.

Region	Metrics				Trends			
	F	*D*	*I*	*M*	*F*	*D*	*I*	*M*
World	2.79	4.93	2.54	35.72	−0.06	−0.04	**−0.04***	**−1.63***
Polar	4.96	5.40	2.79	74.93	**−0.28***	**−0.11***	−0.01	**−5.90***
Cold	3.50	4.94	3.17	55.89	**−0.10***	**−0.12***	**−0.05***	**−4.41***
Arid	2.60	4.66	2.17	26.69	−0.02	−0.01	0.02	0.03
Temperate	1.92	4.37	2.08	17.67	0.04	0.06	−0.03	0.42
Tropical	1.11	4.79	1.26	6.70	0.06	**0.14***	**−0.05***	0.27

Units of *F*, *D*, *I* and *M* are time year^{-1}, day event^{-1}, °C day^{-1} event^{-1}, and °C year^{-1}. Units of trends for *F*, *D*, *I*, and *M* are time decade^{-1}, day event^{-1} decade^{-1}, °C day^{-1} event^{-1} decade^{-1}, and °C decade^{-1}. Trends were estimated for 1980–2018 using Mann-Kendall test and Theil-Sen method, and significant trends at the 5% level were marked with * and in bold.

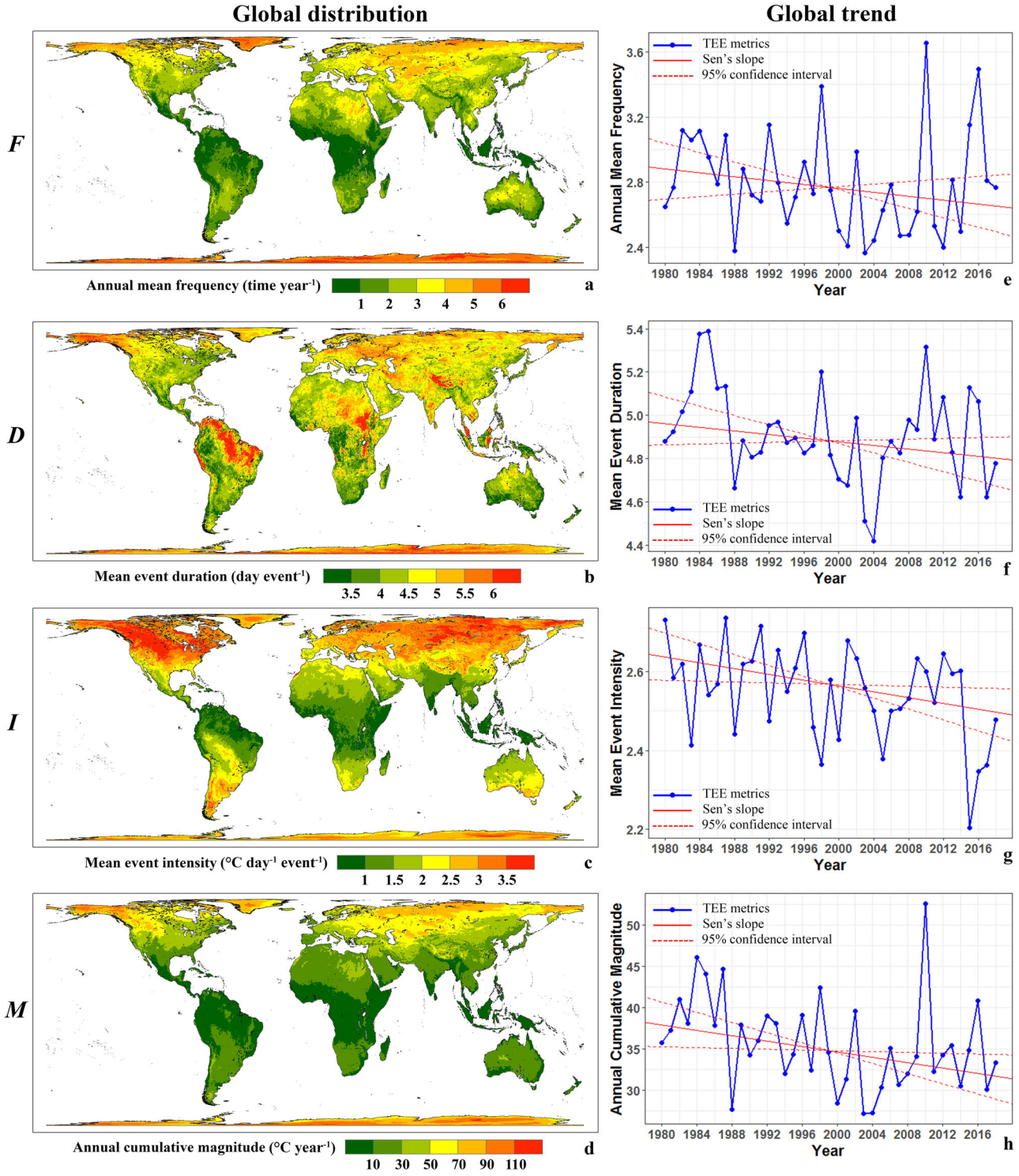

Fig. 1 Global distribution and trends of annual mean frequency (*F*), mean event duration (*D*), mean event intensity (*I*), and annual cumulative magnitude (*M*) for all identified temperature extreme events (TEEs). a–d Global distribution of *F*, *D*, *I* and *M*. **e–h** Global trends of *F*, *D*, *I* and *M*. Trends were estimated for 1980–2018 using Mann–Kendall test and Theil–Sen method.

As the combined effect of opposite heat and cold extreme trends, overall decreasing trends can be observed for the world in all four metrics of TEEs (Fig. 1e–h), with trends in *I* and *M* being statistically significant at the 5% level (Table 1). Significant decreasing trends can be observed for most metrics in the Polar and Cold zones, with the exception of *I* in the Polar zone. There were no significant trends in the Arid and Temperate zones. Trends in the Tropical zone is noteworthy, with significantly increasing *D* and decreasing *I* (Table 1). Spatially, there were no globally consistent trends (Supplementary Fig. S2). The increasing and decreasing trends each constituted about half of the land surface for all four metrics, with decreasing trends' proportion being slightly higher. As for climate zones, increasing trends prevailed in the Tropical and Temperate zones, while decreasing ones prevailed in the Arid, Cold and Polar zones. Much less land area was covered by significant trends (10–15%) (Supplementary

a

TEE Type	Example	Abbreviation
TEEs involving only heat extreme days	H H-H H-H-H H-H-H-H	ALL-H
Single TEEs involving only heat extreme days	H	SINGLE-H
Compound TEEs involving only heat extreme days	H-H H-H-H H-H-H-H	COMP-H
TEEs involving only cold extreme days	C C-C C-C-C C-C-C-C	ALL-C
Single TEEs involving only cold extreme days	C	SINGLE-C
Compound TEEs involving only cold extreme days	C-C C-C-C C-C-C-C	COMP-C
Compound TEEs involving both heat and cold extreme days	H-C C-H H-H-C C-H-C	COMP-HETERO
Single TEEs	H C	SINGLE
Compound TEEs	H-H C-C C-H H-C-H	COMP

b

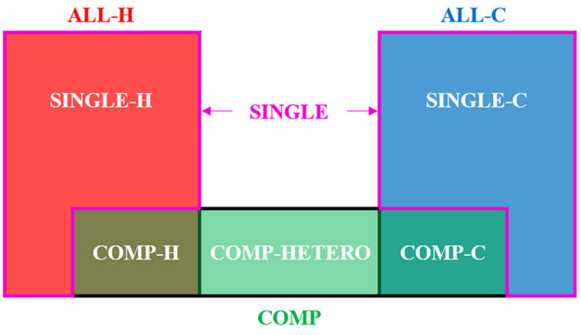

Fig. 2 Major types of temperature extreme events (TEEs). a Examples and abbreviations. **b** A schematic diagram of relationships among major types of TEEs. Individual TEEs involving only heat and cold extreme days are denoted as H and C respectively. Single and compound TEEs were expressed as H and/or C connected by hyphens (e.g., H represents a single TEE, and H-C represents a compound TEE composed of an H followed by a C).

Figs. S2e–h). With heat and cold extremes considered as a whole, patterns and trends of TEE metrics were analysed, which may provide a new perspective for understanding how extreme climate events have been and will be affected by climate change.

Shift towards a heat-extreme-prevailing climate. The patterns and trends of heat extremes as opposed to those of cold extremes remain unclear across the globe. In order to fill the research gap, we focus on the analyses of heat and cold extremes in a comparative manner—TEEs involving only heat and only cold extreme days (ALL-H and ALL-C, see Fig. 2). On average, cold extremes occurred slightly more frequently than heat extremes globally (1.39 vs. 1.36 times year^{-1}), with a higher D (4.81 vs. 4.76 days event^{-1}) and I value (2.60 vs. 2.50 °C day^{-1} event $^{-1}$), resulting in a greater value of M (18.03 vs. 16.40 °C year^{-1}) (Supplementary Table S1).

Figure 3a and b displays the spatial distribution of M for heat and cold extremes, both exhibiting a poleward increasing gradient as influenced by temperature variability patterns. Similar latitudinal gradients were also identified in previous studies for heat and cold extreme frequency[48] and intensity[18,49]. Regions with high values of M (>40 °C year^{-1}) were mostly located in the Arctic and Antarctica for heat extremes (Fig. 3a), and were concentrated in small areas of Antarctica, Alaska, North America along the Rocky Mountains, central and western Russia, and central Asia for cold extremes (Fig. 3b).

We designed a Normalized Difference TEE Index (NDTI) to quantify the difference between M values of heat and cold extremes (see Methods for details of NDTI calculation). NDTI ranges from −1 to 1. Positive and negative values imply heat and cold extremes prevail respectively, and 0 indicates a perfectly balanced state of heat and cold extremes in terms of M. The global average NDTI was −0.05, indicating that heat and cold extremes were roughly balanced, with M of cold extremes being slightly higher. Among five climate zones, heat and cold extremes were proportional in the Temperate zone (NDTI: −0.01); heat extremes prevailed in the Polar and Tropical zones (NDTI: 0.13 and 0.16), while cold extremes prevailed in the Cold and Arid zones (NDTI: −0.15 and −0.16) (Supplementary Table S1).

Spatially, the NDTI revealed distinct heat-extreme- and cold-extreme-prevailing regions (Fig. 3c). Heat extremes prevailed in ~47% and cold extremes in ~53% of land area. About 13% and 5% of land area is heat-extreme- (NDTI > 0.5) and cold-extreme-dominating (NDTI < −0.5). Most (~70%) of the heat-extreme-dominating region was in the Tropical zone, while the cold-extreme-dominating region was largely distributed in the Arid (~42%) and Cold zones (~25%), with hotspots located in western North America, southern Amazon, central Russia, southern Middle East and northwestern Australia (Fig. 3c).

Both F and M had been significantly decreasing for cold extremes (Fig. 4e and h) and significantly increasing for heat extremes globally (Fig. 4a and d). A few studies with a global focus[18,26] also detected the increasing trends of heat extremes in frequency and magnitude, on which a general consensus has been reached[1]. Cold extremes were reported to get milder in some regional studies[7,10,23,38,39,50], and no global conclusions have been drawn yet to our best knowledge. Trends of F and M in all five climate zones were consistent with global ones, except that the increasing trends of heat extremes in the Polar zone were not significant (Supplementary Table S1). Noteworthy trends were exhibited in the event-wise metrics (D and I): Cold extremes had become more intense and significantly shorter (Fig. 4f and g), and heat extremes longer and significantly less intense (Fig. 4b and c).

Globally the decreasing rates of F and M for cold extremes were higher than the corresponding increasing rates for heat extremes (Supplementary Table S1), leading to the downward trend of TEEs (Fig. 1e and h). In previous literature, the comparison of change rates between heat and cold extremes was only limited to a few regions with inconsistent conclusions[10,27–29]. Inconsistent rate difference can also be observed across climate zones in our study. Heat extremes increased faster in the Temperate and Tropical zones, whereas cold extremes decreased faster in the Cold and Polar zones, with comparable change rates in both extremes in the Arid zone (Supplementary Table S1). The difference between heat and cold extreme change rates resulted in, whether significant or not, corresponding expected trends in the F and M of TEEs in respective climate zones (Table 1).

The trends of M in both heat and cold extremes collectively resulted in a significant increase of the global NDTI with 0.23 per decade. The global NDTI had changed from ~ −0.4 to ~0.4 during the study period 1980–2018, indicating that the world had gradually shifted from a cold-extreme- to a heat-extreme-

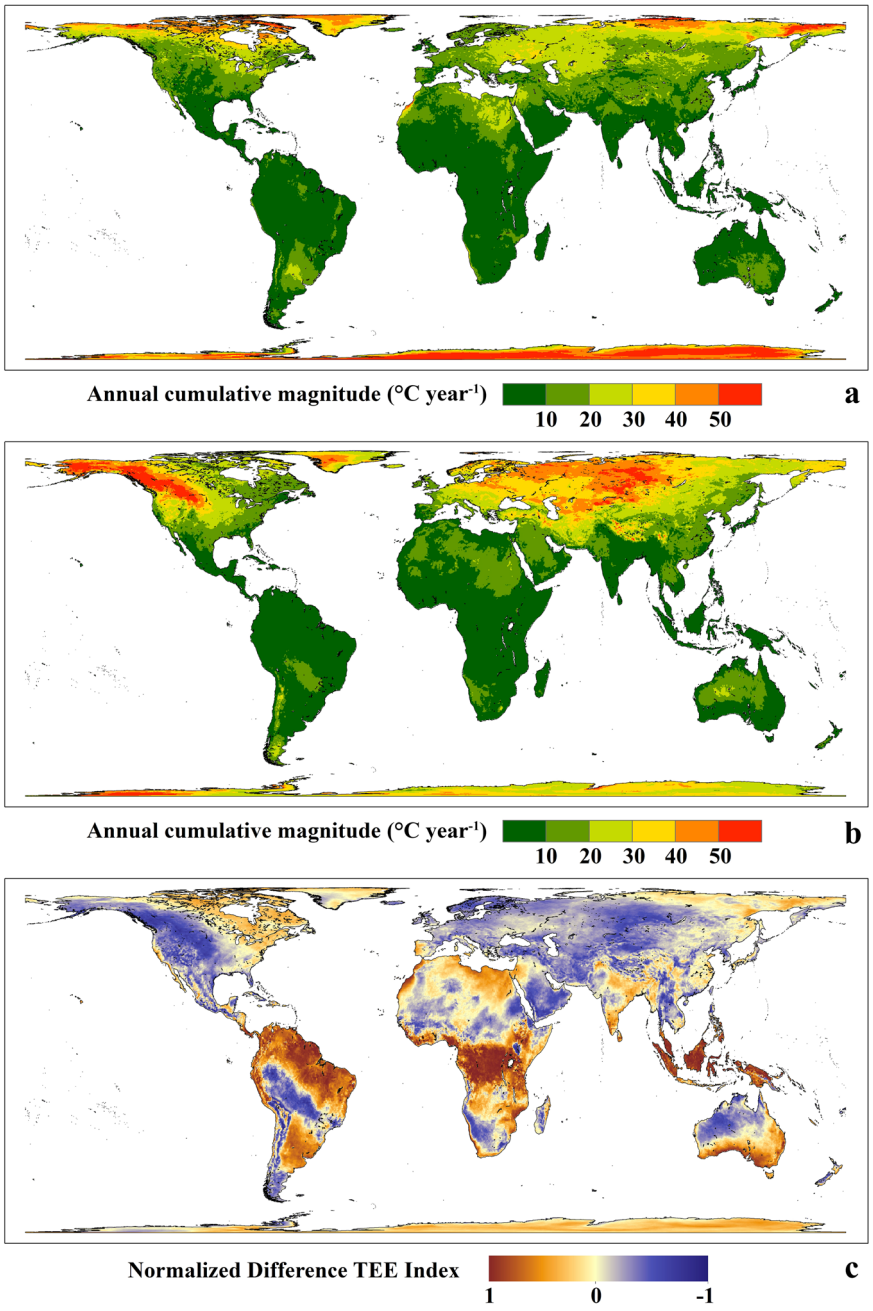

Fig. 3 Global distribution of annual cumulative magnitude (*M*) for heat and cold extremes, and of Normalized Difference TEE Index (NDTI). a *M* of heat extremes. **b** *M* of cold extremes. **c** NDTI.

prevailing climate (Supplementary Fig. S3a). The transition occurred around year 2000 with NDTI values close to 0. The climate regime change was the fastest in the Tropical zone due to pronounced percentage changes of *M* in both heat and cold extremes, and the slowest in the Polar zone with much smaller percentage changes (Supplementary Table S1). Although not directly comparable, quite a few studies noted much larger or earlier increase of heat extremes in the tropics in various metrics due to lower temperature variability[36,40,49,51–55].

Overwhelming proportions of the land surface exhibited an increasing trend in heat extremes and a decreasing trend in cold extremes (89% vs. 92%) in terms of *M* (Fig. 5a and c). The increasing heat extremes and decreasing cold extremes since the 1950s over most of the land surface was identified as "virtually certain" by the IPCC AR6 report[1], for which human-induced greenhouse gas is considered the dominant factor. However, it should be noted that this conclusion in the IPCC AR6 was drawn mostly from metrics based on daily temperatures, such as the Expert Team on Climate Change Detection and Indices (ETCCDI) indices. Our study confirms and reinforces this conclusion using metrics based on explicitly identified TEEs.

The surface area proportion with an increasing trend in heat extremes and that with a decreasing trend in cold extremes were both greater than 90% in most climate zones. An exception was the Polar zone, only 62% of which was characterized by increasing heat extremes and 84% by decreasing cold extremes. About half of land surface had experienced significantly increasing heat extremes and significantly decreasing cold extremes respectively (47% vs. 45%) (Fig. 5b and d). Consistent with a previous study[18], there was a vast area in the central and

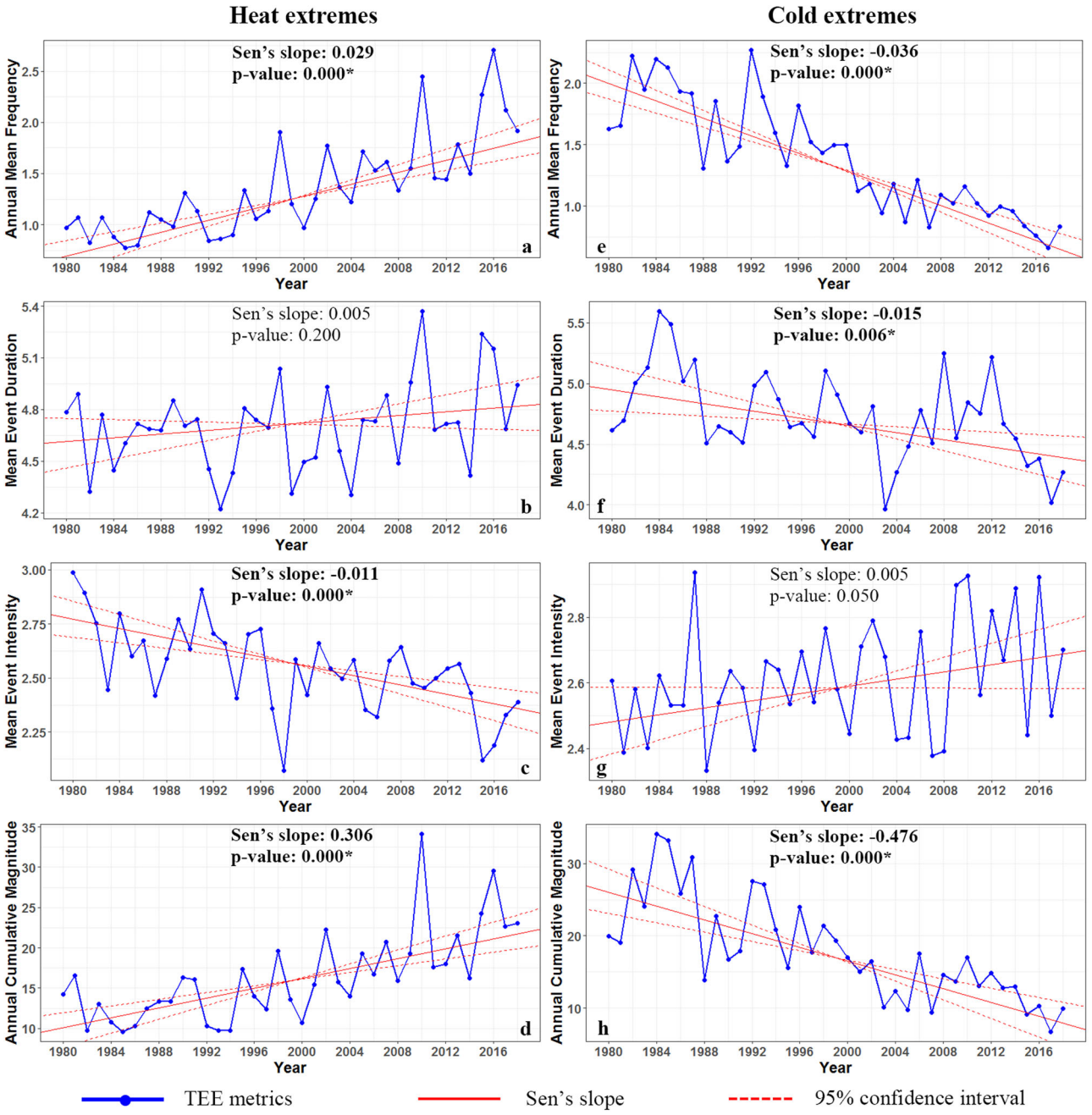

Fig. 4 Global trends of heat and cold extremes. a–d Trends of annual mean frequency (*F*), mean event duration (*D*), mean event intensity (*I*) and annual cumulative magnitude (*M*) for heat extremes. **e–h** Trends of *F*, *D*, *I* and *M* for cold extremes. Trends were estimated for 1980–2018 using Mann–Kendall test and Theil–Sen method, and significant trends at the 5% level were marked with * and in bold.

southeast US without significant trends of *M* for heat extremes (Fig. 5b), due to the existence of warming hole around this area[56,57]. The IPCC AR6 report also identified two AR6 regions (Central North America and Eastern North America) as having "low agreement in the type of change" for heat extremes[1]. The *M* of heat extremes increased the fastest in the Arctic region, and the increasing trend was also very pronounced in regions around the Caspian Sea and north of the Black Sea (Fig. 5b). The *M* of cold extremes decreased the fastest in the Cold zone in northern Russia, Alaska, and northwestern Canada, with noteworthy decreasing trends observed in the mid-US, northern Africa and south of the Caspian and Black Sea (Fig. 5d).

Analysing heat and cold extremes in a comparative manner enabled us to examine the spatial distribution of different combinations of their trends, which hasn't been explored previously. Different directions of trends in *M* values of heat and cold extremes resulted in four types of trend combinations. As shown in Fig. 5e, an overwhelming majority of land surface (>80%) exhibited increasing heat extremes and decreasing cold extremes simultaneously globally and in most climate zones. The exception was the Polar zone, only 55% of which exhibited such trend. Another 29% of the Polar zone experienced an observed decreasing trend of both heat and cold extremes, which can also be observed in North America. The increasing trend of both heat and cold extremes was exhibited in central Asia, and small areas in Australia and South America, with 40% of the regions concentrated in the Arid zone. The trend combination of decreasing heat extremes and increasing cold extremes, opposite

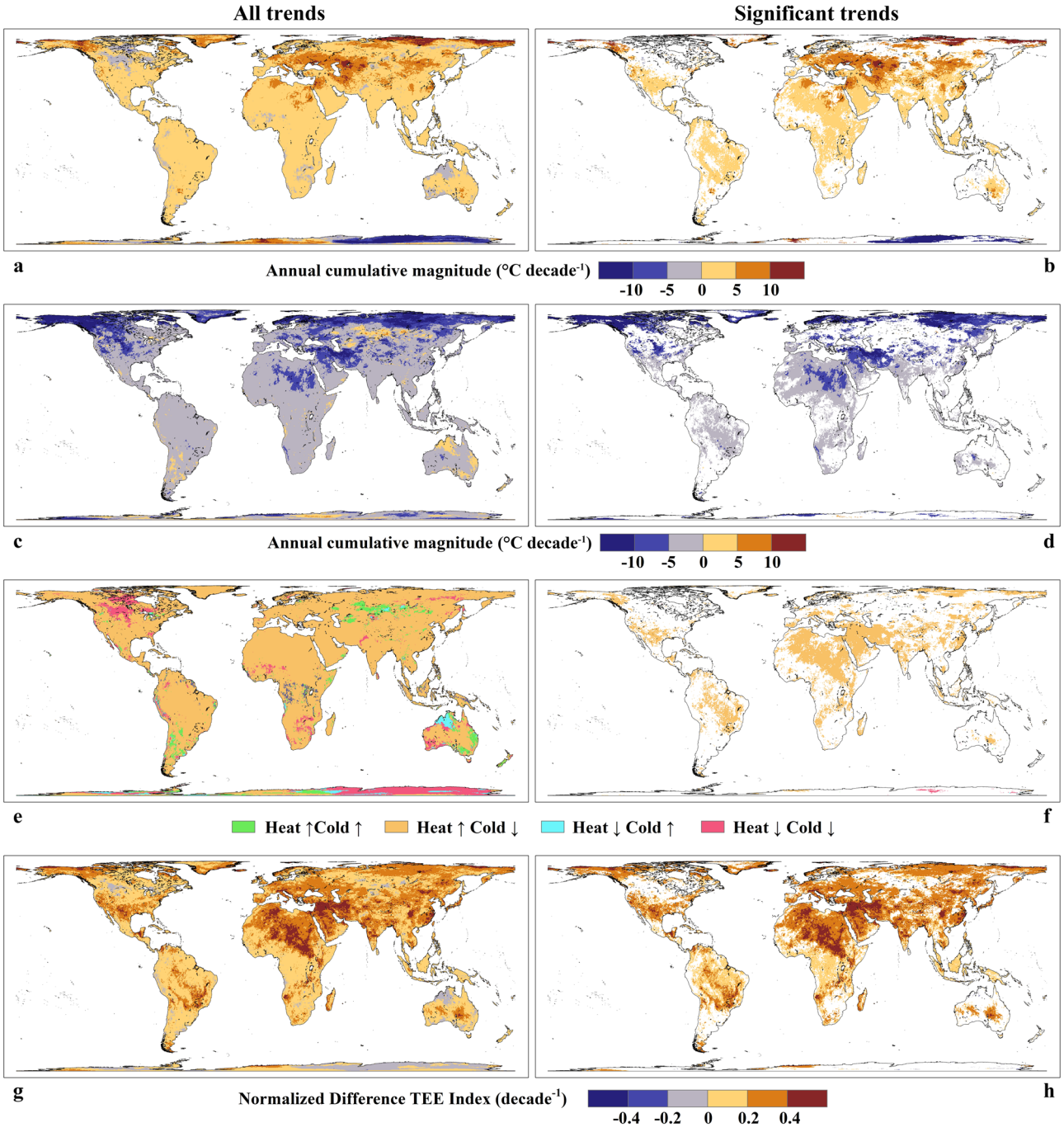

Fig. 5 Global distribution of temporal trends for heat and cold extremes. a, **b** Trends of annual cumulative magnitude (*M*) for heat extremes. **c**, **d** Trends of *M* for cold extremes. **e**, **f** Classes of trend combinations. **g**, **h** Trends of Normalized Difference TEE Index (NDTI). Trends were estimated for 1980–2018 using Mann–Kendall test and Theil–Sen method, and **b**, **d**, **f**, and **h** show only significant trends at the 5% level.

to the dominating trend combination, was the least common, with only small areas distributed mainly in northwestern Australia and Antarctica.

Significant trend combinations were predominantly increasing heat extremes and decreasing cold extremes, covering 26% of the land surface (Fig. 5f). Regions experiencing such trend were concentrated in the Arid zone, with noticeable contiguous regions in the Middle East and North Africa (MENA). Only a negligible proportion (<0.2%) showed other significant trends (Fig. 5f). Due to spatio-temporal variation and heterogeneity of TEE dynamics as influenced by climate change, heat extremes increased faster than cold extremes decreased in some parts of the world (7%) while in others (15%) cold extremes decreased faster, producing an interwoven pattern (Supplementary Fig. S4). Change rates between heat and cold extremes have only been compared in a few regions, such as the Northeastern US[10,27,28] and Korea[29]. Although the TEE definition and metrics may differ, the spatio-temporal patterns revealed by our grid-cell-based comparison (Supplementary Fig. S4) are roughly consistent with their regional conclusions, yet with greater spatial details.

The NDTI trend (Fig. 5g and h) quantitatively reveals the difference between the trends of *M* in heat and cold extremes from a different perspective. Most of the globe had changed towards a heat-extreme-prevailing climate regime, with 92% of

the land surface exhibiting an increasing trend of NDTI (Fig. 5g), and 60% covered by significantly increasing NDTI (Fig. 5h). Regions of rapid significant NDTI increase (>0.2 per decade) corresponded very well with those of both significant heat extreme increasing and cold extreme decreasing trends (Fig. 5f and h). This demonstrates that both the increasing heat extremes and decreasing cold extremes contributed to the climate regime shift. The most rapid NDTI increase was concentrated in the MENA region, and in a few isolated areas of East Asia. The MENA region, including the Mediterranean region, is regarded as one of the most prominent climate change hotspots[58,59]. This is confirmed in Fig. 5, with MENA featured by high heat extreme increasing, cold extreme decreasing and NDTI increasing rates. The dramatic past and projected heat extreme increases in the MENA have also been highlighted in a number of recent studies, for which reduced precipitation, depleted soil moisture, and elevated greenhouse gas concentration were considered responsible[18,36,52,54,60–62].

Percentage and composition of compound TEEs. The comparison of *F* and *M* between compound TEEs and all identified TEEs reveals that although only one out of ten TEEs were compound ones, they accounted for about a quarter of TEE magnitude globally. Compound TEEs generally have longer duration and lower intensity than single TEEs, because break durations were considered (see Methods for details of TEE metric calculation). Thus, the spatio-temporal variation in their percentage can potentially influence the metrics of *D* and *I*. In view of compound TEEs' significance, we first focus on analysing the percentage of compound TEEs out of all identified TEEs in terms of *M* (i.e., compound percentage). Regions of high compound percentage were predominantly in the Tropical zone (Fig. 6a). Notable hotspots coincided with regions of longer *D* (Fig. 1b), implying that the greater compound percentage is a major reason of prolongation of *D*.

Compound TEEs can involve only heat extreme days (COMP-H), only cold extreme days (COMP-C) or both (COMP-HETERO) (see Fig. 2 for details of abbreviations). Figure 6b displays the distribution of the dominating compound TEE type and the compound TEE composition in different climate zones. Same-type compound TEEs (COMP-H and COMP-C) dominated over ~86% of the land surface, while only 5% showed COMP-HETERO dominance, distributed mainly in southeastern China and northeastern Russia. The composition of compound TEE in terms of *M* was similar in the Polar and Temperate zones, with a roughly balanced proportion of COMP-H and COMP-C, and a higher COMP-HETERO proportion (~20%) relative to other climate zones (Fig. 6b). A greater proportion of COMP-C than COMP-H was found in the Cold and Arid zones, where the COMP-HETERO proportion was around 10%. The composition in the Tropical zone is notable, with a very small proportion of COMP-HETERO (3%), and a much greater proportion of COMP-H (81%) compared to COMP-C (16%).

We also focused on the heat and cold extremes, respectively, and analysed the percentage of COMP-H (COMP-C) out of ALL-H (ALL-C) in terms of *M* (i.e., COMP-H and COMP-C percentages). Regions with a high COMP-H percentage were widely distributed in the Tropical zone (Fig. 6c), while those with a high COMP-C percentage concentrated around the Black and Caspian Sea, and on the Tibetan Plateau (Fig. 6d).

The compound percentage exhibited a significant decreasing trend globally at −0.87% per decade, and varied across climate zones (Table 2). Significant trends can only be observed in the Cold and Tropical zones, with change rates of −2.03% and 4.26% per decade, respectively. The considerable compound percentage increase in the Tropical zone potentially resulted in significantly increased *D* and decreased *I* (Table 1). COMP-H had gradually become the dominant compound TEE type globally and in all climate zones, as the collective effect of significantly increasing proportions of COMP-H and decreasing proportions of COMP-C in compound TEEs (Table 2).

The COMP-H and COMP-C percentages exhibited increasing and decreasing trends (Table 2), which are considered a major cause of the trends in global average *D* and *I* of heat and cold extremes, respectively (Fig. 4b, c and f, g). The decrease in COMP-C percentage was significant globally and across all climate zones. The increase in COMP-H percentage was only significant in the Temperate and Tropical zones, with the greatest increase rates observed in the Tropical zone. The trends in COMP-H and COMP-C percentages can be explained by the upward shift of global mean temperature, which can cause higher (lower) probability to surpass (fall below) the 90th (10th) percentile thresholds (see Methods for TEE definition)[40]. The stable temperature variability in the Tropical zone makes it easier to exceed heat extreme thresholds as the climate warms, resulting in the greatest increase of COMP-H percentage. A previous study[40] noted that the proportion of compound heatwave days increased under global warming, and the greatest increase was found to be in the tropics, consistent with our findings.

Compound extreme events are associated with greatly amplified impacts, the research into which is crucial for improved risk assessment and management[41]. The proper analysis and improved understanding of compound TEEs, an important type of temporally compounding events, are still lacking with only very few related research[40]. To the best of our knowledge, our analysis exhibited the spatial patterns and temporal trends of compound TEE percentages and composition for the first time. It reveals that globally the compound TEE percentage significantly decreased possibly associated with the faster decrease of COMP-C percentage than the increase of COMP-H percentage, whereas the chance of other compound extreme events (e.g., concurrent heat waves and droughts, and compound flooding) was reported to have increased either at global or regional scales[1].

Conclusions. TEEs have caused catastrophic impacts on human health, economy and environment[10,12,17,18]. Understanding TEE dynamics as influenced by climate change is therefore of utmost importance for effective response and adaptation. We analysed the spatio-temporal characteristics of TEEs at the global scale, considering their compounding and using unified TEE definitions and metrics. Over the study period 1980–2018, the *M* of heat extremes significantly increased at 3.06 °C decade^{-1}, while that of cold extremes decreased at −4.76 °C decade^{-1}, on global average. Consequently, the world had transformed rapidly and steadily from a cold-extreme- to a heat-extreme-prevailing climate, as indicated by the change of NDTI from ~ −0.4 to ~0.4 at a significant rate of 0.23 per decade. Contrary to general belief, TEEs as a whole had become significantly milder globally with a decreasing rate of −1.63 °C decade^{-1} in *M*, due to the faster decrease in cold extremes compared to the increase of heat extremes. The compound percentage had marginally, yet significantly decreased by 0.87% per decade, resulting in evident spatio-temporal variation of *D* and *I*.

Overall, these trends were not globally uniform. For example, the decreasing trend of TEEs in *M* can only be observed over a little more than half (and significantly decreasing trend only over 9%) of the land surface area, despite the significant global decreasing trend. The trends of heat extremes (Fig. 5a and b), cold extremes (Fig. 5c and d) and their trend combinations (Fig. 5e and f) also exhibited pronounced spatial heterogeneity. The MENA region stood out as a hotspot of shift towards a heat-extreme-prevailing climate, with fast and significant heat extreme

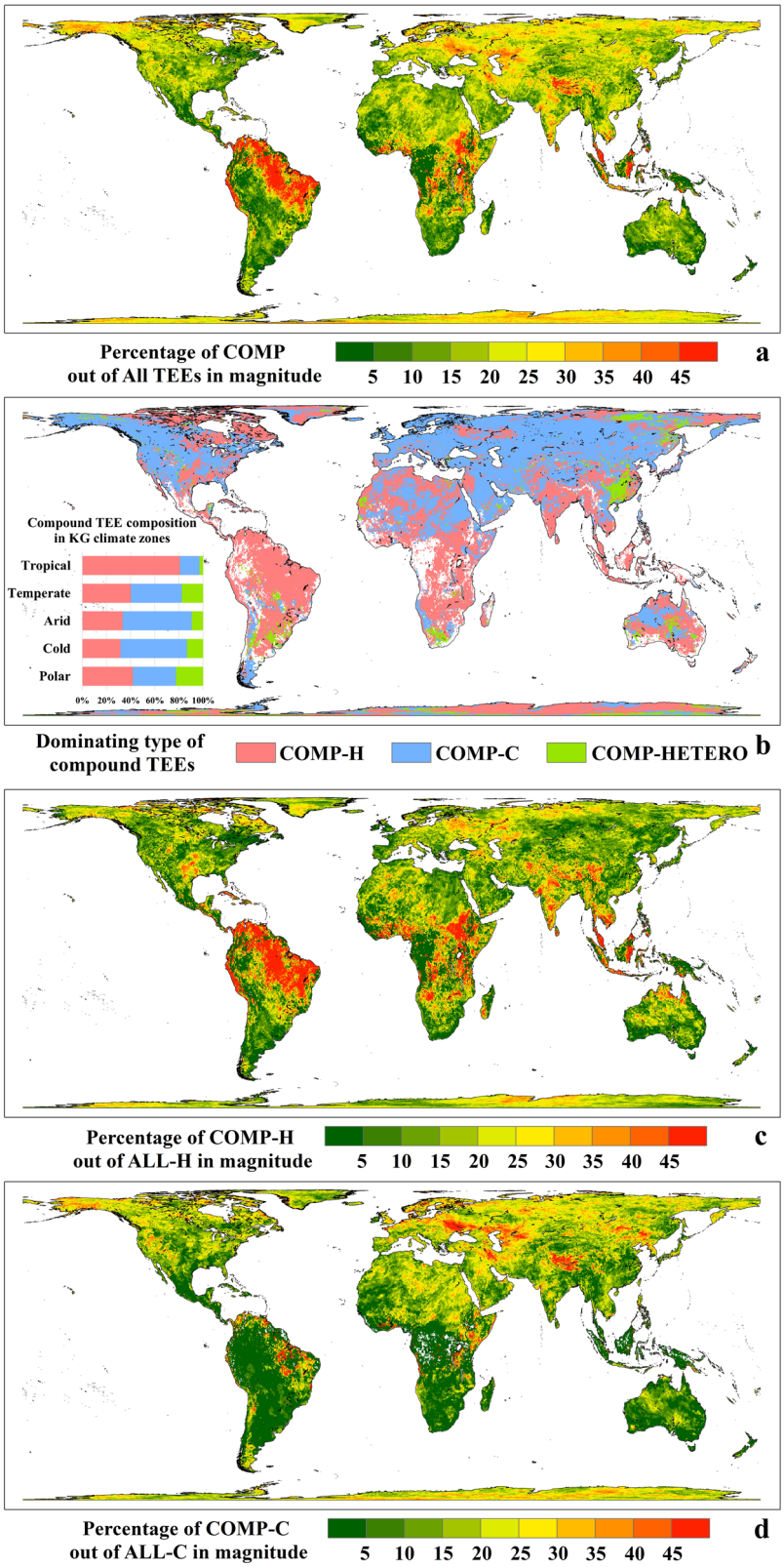

Fig. 6 Global distribution of compound temperature extreme event (TEE) percentages. a Percentage of compound TEEs out of all identified TEEs in annual cumulative magnitude (*M*). **b** Compound TEE composition. **c** Percentage of COMP-H out of ALL-H in *M*. **d** Percentage of COMP-C out of ALL-C in *M*. Figure 2 lists abbreviations of major types of TEEs.

Table 2 Global and regional trends of compound temperature extreme event (TEE) percentage and composition.

	Compound percentage	Compound TEE composition			COMP-H percentage	COMP-C percentage
		COMP-H	COMP-C	COMP-HETERO		
World	−**0.87***	**12.55***	−**12.06***	−0.54	0.95	−**2.28***
Polar	−0.82	**6.52***	−**7.63***	0.54	0.25	−**2.31***
Cold	−**2.03***	**13.09***	−**12.08***	−1.16	0.74	−**2.66***
Arid	−0.51	**15.84***	−**16.27***	1.22	1.53	−**2.32***
Temperate	0.19	**17.38***	−**19.78***	1.40	**2.42***	−**2.69***
Tropical	**4.26***	**16.23***	−**16.14***	−0.65	**2.57***	−**1.94***

Trends were estimated for 1980–2018 using Mann–Kendall test and Theil–Sen method, and significant trends at the 5% level were marked with * and in bold. Units are % decade^{-1}.

increase, cold extreme decrease and NDTI increase. As a result of global heterogeneity, different patterns and trends were identified among climate zones, and the most noteworthy is in the Tropical and Polar zones.

The shift towards a heat-extreme-prevailing climate regime was the fastest in the Tropical zone (NDTI increase rate: 0.40 per decade), due to the fast percentage changes of heat (32% decade^{-1}) and cold extremes in M (−36% decade^{-1}). The Tropical zone was also associated with the most rapid increase of compound TEE percentage (4.26% decade^{-1}), resulting in significantly increased D and decreased I of TEEs. Unlike global trends, TEEs as a whole had become slightly more severe (M change rate: 0.27 °C decade^{-1}) in the Tropical zone, though not significant. Conversely, TEEs had become significantly milder (M change rate: −5.90 °C decade^{-1}), and the climate regime shift was the slowest in the Polar zone (NDTI increase rate: 0.12 per decade) due to the lowest percentage changes of heat (2% decade^{-1}) and cold extremes in M (−22% decade^{-1}). The globally dominating trend of increasing heat extremes and decreasing cold extremes was the most uncommon in the Polar zone, with only 55% covered by such trends, in contrast to >80% in other climate zones.

Compared with prior studies with only a regional focus[10,27–29,37,45,49,51,63–65] or on only limited types of TEEs (mostly heat waves)[18,26,40,46,54,66], our analysis provided a panoramic view of global patterns and trends of TEEs with both heat and cold extremes considered, of heat vs. cold extremes, and of compound TEEs. We also revealed greater spatial details and heterogeneity by adopting the high spatio-temporal resolution ERA5 data. The enhanced understanding of global and regional TEE patterns and trends provided new insights to support more oriented, effective and localized adaptation to climate change. Our results were based solely on ERA5 due to the limited availability of high quality, long term, and fine spatio-temporal resolution climate data. We used a fixed threshold of break durations to define compound TEEs, while locally adjusted thresholds are expected to better account for the spatially variant time span of TEE influence dependent on local climate conditions and adaptability. However, our analytical framework (including TEE definition, classification, extraction, metrics, and analysis) is a pioneer effort towards the establishment of a unified framework to measure and analyse TEEs, the need for which has been identified in a few studies[36]. Upon availability of other eligible data, similar analysis can be conducted to validate our findings. The framework can also be applied to ESM projections to analyse future patterns and trends of TEEs under different climate change scenarios.

Methods

ERA5 reanalysis dataset. The hourly air temperature at 2 m over the period 1980–2018 was acquired for the globe from the European Centre for Medium–Range Weather Forecasts (ECMWF) Reanalysis 5 (ERA5) product[67]. Daily maximum (T_{max}) and minimum air temperature (T_{min}) were calculated from the ERA5 dataset for the derivation of TEEs, and reprojected to the Behrmann equal area projection with a resolution of 25 km (~0.25° at the equator).

Definition of individual TEEs. No consensus has been achieved regarding the definitions of TEEs[12,21,36]. To account for the acclimatization to local climate, percentile-based thresholds have gradually replaced absolute thresholds[37,68], thus enabling inter-region comparison for global studies[69]. In this sense, TEEs have been defined in previous studies[26,45,46,54] as prolonged excessive heat or cold beyond percentile-based thresholds. Such daily thresholds were calculated relative to the region of interest over a temporal window, in order to be spatially and seasonally specific. These TEE definitions used varying temperature variables (e.g., T_{max}, T_{min} and apparent temperature (T_a)), percentile values (e.g., 5th, 10th, 90th and 95th), minimum duration requirements (e.g., 3, 5 and 6 days), and temporal window lengths (e.g., 15 and 31 days).

In this study, thresholds for both T_{max} and T_{min} were considered[48,70–72], and the percentile values were set to 90th for heat extremes and 10th for cold extremes. The 90th and 10th percentile thresholds were calculated at each grid cell for each calendar day over a 15-day window centred on the day of interest for the reference period 1980–2018. Periods of at least 3 consecutive days with both T_{max} and T_{min} higher than their respective 90th percentile were identified as heat extreme days. Cold extreme days were identified in a similar way, but with T_{max} and T_{min} lower than the 10th percentile. An individual TEE is defined as a period of consecutive heat or cold extreme days.

Definitions of single and compound TEEs. When extreme events occur consecutively, it is indicated that individuals, economic sectors or ecosystems become more vulnerable to the subsequent event(s) during the recovery time from the previous one(s), leading to amplified societal or ecological impacts[40,43,44]. Extreme events occurred sequentially are therefore considered not dependent or temporally compounding. Temporally compounding events represent an important type of compound events, which also include preconditioned, multivariate and spatially compounding events[41].

Sequences of individual TEEs are a typical example of temporally compounding events. Since the effects of temperature on mortality are largely concentrated within a week[73], here we define a compound TEE (COMP) as a succession of individual TEEs separated by breaks shorter than 7 days. A compound TEE can involve two or more individual TEEs of the same type or different types. An individual TEE that is not part of any compound TEEs is defined as a single TEE (SINGLE).

Nine non-mutually-exclusive types of TEEs can be identified (Fig. 2). TEEs can be divided into SINGLEs and COMPs dependent on the number of individual TEEs involved. They can also be divided into TEEs involving only heat extreme days (ALL-Hs), involving only cold extreme days (ALL-Cs) and involving both (COMP-HETEROs), from a different perspective of individual TEE types. ALL-Hs can be further classified into single (SINGLE-Hs) and compound TEEs involving only heat extreme days (COMP-Hs), and ALL-Cs into SINGLE-Cs and COMP-Cs likewise. A schematic diagram is provided to visualize relationships among these TEE types (Fig. 2b).

TEE extraction at the grid cell scale. Following the TEE definitions, individual TEEs were first extracted based on the daily T_{max} and T_{min} of the ERA5 dataset, without considering their compounding. Individual TEEs were extracted at the grid cell scale over the period of 1980–2018. TEEs occurring during the entire year were considered rather than only in summer or warm season for heat extreme days and only in winter or cold season for cold extreme days, so that different types of TEEs (heat waves, warm spells, cold waves and cold spells) can be included in the analysis.

For each grid cell, sets of individual TEEs in succession with their break durations <7 days were identified and combined to form separate compound TEEs; the other individual TEEs left unchanged were identified as single TEEs. Individual TEEs were thus transformed into single and compound TEEs at the grid cell scale for further analysis.

Attributes of a TEE. Each identified single or compound TEE is associated with five attributes: location (grid cell), timing (date of occurrence), type (see Fig. 2), duration, and intensity. The first three attributes are self-explanatory. A TEE's duration (d) is the number of days it lasts, with break durations included for compound TEEs. The

intensity (i) of a TEE is the average daily extra heat and/or cold suffered during the TEE:

$$i = \frac{\sum_{k=1}^{d} \triangle T_k}{d} \quad (1)$$

where i and d are the intensity and duration of the TEE, and $\triangle T_k$ is the temperature anomaly on day k of the TEE. $\triangle T_k$ is calculated as T_{max} anomaly relative to the calendar-day 90th percentile for heat extreme days, as T_{min} anomaly relative to the 10th percentile for cold extreme days, and is 0 for break durations.

TEE metrics at the grid cell, regional and global scales. Four metrics of annual mean frequency (F), mean event duration (D), mean event intensity (I), and annual cumulative magnitude (M) were calculated for multiple TEEs involved at the grid cell, regional and global scales, for the assessment of the spatial patterns and temporal trends of TEEs.

The four metrics were originally calculated at the grid cell scale. F (unit: time year^{-1}) is the average number of TEEs occurring per year. D (unit: day event^{-1}) and I (unit: °C day^{-1} event^{-1}) are both event-wise metrics and were calculated as the average duration and intensity of the TEEs involved:

$$D = \frac{\sum_{e=1}^{F\times y} d_e}{F\times y} \quad (2)$$

$$I = \frac{\sum_{e=1}^{F\times y} i_e}{F\times y} \quad (3)$$

where d_e and i_e are the duration and intensity of the TEE e, y is the number of years in the period of interest, and $F\times y$ is the number of TEEs involved. M (unit: °C year^{-1}) is the average extra heat and/or cold accumulated annually, and was calculated as:

$$M = \frac{\sum_{e=1}^{F\times y}\sum_{k=1}^{d_e} \triangle T_k}{y} \quad (4)$$

Equation (4) can also be written as:

$$M = \frac{\sum_{e=1}^{F\times y} i_e \times d_e}{y} \quad (5)$$

TEE metrics were then calculated for five KG climate zones and for the world. F and M at the regional and global scales were calculated as the spatial mean of all grid cells involved. D and I at the regional and global scales were calculated as:

$$D_R = \frac{\sum_{c\in \boldsymbol{C}} D_c \times F_c}{\sum_{c\in \boldsymbol{C}} F_c} \quad (6)$$

$$I_R = \frac{\sum_{c\in \boldsymbol{C}} I_c \times F_c}{\sum_{c\in \boldsymbol{C}} F_c} \quad (7)$$

where D_R and I_R are regional and global D and I, respectively, $\boldsymbol{C}$ is the set of grid cells within respective climate zones or the world, D_c, I_c and F_c are the D, I and F values of grid cell c within the set $\boldsymbol{C}$.

Pattern and trend analysis. We performed three series of analyses, focusing respectively on TEEs with both heat and cold extremes considered, the comparison of heat and cold extremes, and compound TEE percentage and composition. In each series of analyses, TEE metrics (F, D, I and M) and their trends were examined and presented at the grid cell, regional and global scales, with greater emphasis placed on M. M can reflect variations in the other three metrics. According to Eq. (5), greater F and/or D result in longer exposure time to TEEs, and greater I result in exposure to increased amount of excess heat and/or cold during the same period of time. Therefore, M is a comprehensive metric indicative of the overall exposure to extreme temperatures and overall TEE severity[18,55].

The non-parametric Mann–Kendall test[74,75] is known to be more robust to data distribution and outliers. The standard two-tailed Mann–Kendall test was used to detect if there's monotonic temporal trends significant at the 5% level in annual TEE metrics at all scales. The Hamed and Rao Modified Mann–Kendall test[76] was used instead in case of autocorrelation. Slopes of the Mann–Kendall trends, the TEE metrics change rates, were estimated using Theil–Sen estimator[77].

We focused on ALL-H and ALL-C events (see Fig. 2 for information on major types of TEEs) to analyse heat and cold extremes in a comparative manner. In addition to four TEE metrics, a Normalized Difference TEE Index (NDTI) was developed to quantify the difference between the M values of ALL-H and ALL-C events:

$$\mathrm{NDTI} = \frac{M_{\mathrm{ALL-H}} - M_{\mathrm{ALL-C}}}{M_{\mathrm{ALL-H}} + M_{\mathrm{ALL-C}}} \quad (8)$$

where $M_{\mathrm{ALL-H}}$ and $M_{\mathrm{ALL-C}}$ are the M values of ALL-H and ALL-C events. NDTI ranges from −1 to 1, with −1 indicating 100% ALL-C, 1 indicating 100% ALL-H, and 0 indicating balanced ALL-H and ALL-C, all in terms of M. When calculating regional and global NDTI, the $M_{\mathrm{ALL-H}}$ and $M_{\mathrm{ALL-C}}$ in Eq. (8) should be the sum of respective metrics over all grid cells within corresponding regions.

In compound TEE analysis, we paid attention to the percentages of compound TEEs (i.e., the percentage of compound TEEs out of all identified TEEs, COMP-H out of ALL-H, and COMP-C out of ALL-C), and compound TEE composition (i.e., the percentages of COMP-H, COMP-C and COMP-HETERO in compound TEEs), all in terms of M.

Data availability

ERA5 data that support the findings of this study are publicly available at https://cds.climate.copernicus.eu/ with the identifier https://doi.org/10.24381/cds.adbb2d47 [67].

Code availability

The code used to analyse the ERA5 data is available from the first author upon reasonable request.

Received: 14 September 2021; Accepted: 3 March 2022;
Published online: 01 April 2022

References

1. IPCC Climate Change 2021: The Physical Science Basis. *Contribution of Working Group I to the Sixth Assessment Report of the Intergovernmental Panel on Climate Change* (Cambridge University Press, 2021).
2. Dosio, A. Projection of temperature and heat waves for Africa with an ensemble of CORDEX Regional Climate Models. *Clim. Dyn.* **49**, 493–519 (2017).
3. Blöschl, G. et al. Changing climate both increases and decreases European river floods. *Nature* **573**, 108–111 (2019).
4. Cid, A. et al. Long-term changes in the frequency, intensity and duration of extreme storm surge events in southern Europe. *Clim. Dyn.* **46**, 1503–1516 (2016).
5. Field, C. B., Barros, V., Stocker, T. F. & Dahe, Q. *Managing the Risks of Extreme Events and Disasters to Advance Climate Change Adaptation: Special Report of the Intergovernmental Panel on Climate Change* (Cambridge University Press, 2012).
6. Horton, D. E. et al. Contribution of changes in atmospheric circulation patterns to extreme temperature trends. *Nature* **522**, 465–469 (2015).
7. Kuang, X., Zhang, Y., Wang, Z., Huang, D. & Huang, Y. Characteristics of boreal winter cluster extreme events of low temperature during recent 35 years and its future projection under different RCP emission scenarios. *Theor. Appl. Climatol.* **138**, 569–579 (2019).
8. Rahmstorf, S. & Coumou, D. Increase of extreme events in a warming world. *Proc. Natl Acad. Sci. USA* **108**, 17905 (2011).
9. Schär, C. et al. The role of increasing temperature variability in European summer heatwaves. *Nature* **427**, 332–336 (2004).
10. Winter, J. M., Bowen, F. L., Partridge, T. F. & Chipman, J. W. Future extreme event risk in the rural Northeastern United States. *Ann. Am. Assoc. Geogr.* **109**, 1110–1130 (2019).
11. Rusticucci, M. Observed and simulated variability of extreme temperature events over South America. *Atmos. Res.* **106**, 1–17 (2012).
12. Brown, S. J. Future changes in heatwave severity, duration and frequency due to climate change for the most populous cities. *Weather Clim. Extremes* **30**, 100278 (2020).
13. Feudale, L. *Large Scale Extreme Events In Surface Temperature During 1950–2003: An Observational And Modeling Study* (George Mason University, 2006).
14. Kong, Q., Guerreiro, S. B., Blenkinsop, S., Li, X.-F. & Fowler, H. J. Increases in summertime concurrent drought and heatwave in Eastern China. *Weather Clim. Extremes* **28**, 100242 (2020).
15. Krueger, O., Hegerl, G. C. & Tett, S. F. B. Evaluation of mechanisms of hot and cold days in climate models over Central Europe. *Environ. Res. Lett.* **10**, 014002 (2015).
16. Lopez, H. et al. Early emergence of anthropogenically forced heat waves in the western United States and Great Lakes. *Nat. Clim. Change* **8**, 414–420 (2018).
17. Parente, J., Pereira, M. G., Amraoui, M. & Fischer, E. M. Heat waves in Portugal: current regime, changes in future climate and impacts on extreme wildfires. *Sci. Total Environ.* **631–632**, 534–549 (2018).
18. Perkins-Kirkpatrick, S. E. & Lewis, S. C. Increasing trends in regional heatwaves. *Nat. Commun.* **11**, 3357 (2020).
19. Ullah, S. et al. Observed changes in temperature extremes over China–Pakistan Economic Corridor during 1980–2016. *Int. J. Climatol.* **39**, 1457–1475 (2019).
20. Harrington, L. J. & Otto, F. E. L. Reconciling theory with the reality of African heatwaves. *Nat. Clim. Change* **10**, 796–798 (2020).
21. Jones, B., Tebaldi, C., O'Neill, B. C., Oleson, K. & Gao, J. Avoiding population exposure to heat-related extremes: demographic change vs climate change. *Clim. Change* **146**, 423–437 (2018).

22. Pachauri, R. K. et al. *Climate Change 2014: Synthesis Report. Contribution of Working Groups I, II and III to the Fifth Assessment Report of the Intergovernmental Panel on Climate Change* (IPCC, 2014).
23. Kim, Y. & Lee, S. Trends of extreme cold events in the central regions of Korea and their influence on the heating energy demand. *Weather Clim. Extremes* **24**, 100199 (2019).
24. Vuille, M., Franquist, E., Garreaud, R., Lavado Casimiro, W. S. & Cáceres, B. Impact of the global warming hiatus on Andean temperature. *J. Geophys. Res.: Atmos.* **120**, 3745–3757 (2015).
25. Falvey, M. & Garreaud, R. D. Regional cooling in a warming world: recent temperature trends in the southeast Pacific and along the west coast of subtropical South America (1979–2006). *J. Geophys. Res.: Atmos.* **114**, D04102 (2009).
26. Perkins, S. E., Alexander, L. V. & Nairn, J. R. Increasing frequency, intensity and duration of observed global heatwaves and warm spells. *Geophys. Res. Lett.* **39**, L20714 (2012).
27. Ning, L., Riddle, E. E. & Bradley, R. S. Projected changes in climate extremes over the Northeastern United States. *J. Clim.* **28**, 3289–3310 (2015).
28. Thibeault, J. M. & Seth, A. Changing climate extremes in the Northeast United States: observations and projections from CMIP5. *Clim. Change* **127**, 273–287 (2014).
29. Choi, G. & Lee, D. E. Changing human-sensible temperature in Korea under a warmer monsoon climate over the last 100 years. *International J. Biometeorol.*, 1–10, https://doi.org/10.1007/s00484-020-01862-8 (2020).
30. Alexander, L. V. & Arblaster, J. M. Assessing trends in observed and modelled climate extremes over Australia in relation to future projections. *Int. J. Climatol.* **29**, 417–435 (2009).
31. Baldi, M., Dalu, G., Maracchi, G., Pasqui, M. & Cesarone, F. Heat waves in the Mediterranean: a local feature or a larger-scale effect? *Int. J. Climatol.* **26**, 1477–1487 (2006).
32. Boschat, G. et al. Large scale and sub-regional connections in the lead up to summer heat wave and extreme rainfall events in eastern Australia. *Clim. Dyn.* **44**, 1823–1840 (2015).
33. Fischer, E. M. & Schär, C. Consistent geographical patterns of changes in high-impact European heatwaves. *Nat. Geosci.* **3**, 398–403 (2010).
34. Frich, P. et al. Observed coherent changes in climatic extremes during the second half of the twentieth century. *Clim. Res.* **19**, 193–212 (2002).
35. Keellings, D. & Waylen, P. Increased risk of heat waves in Florida: characterizing changes in bivariate heat wave risk using extreme value analysis. *Appl. Geogr.* **46**, 90–97 (2014).
36. Perkins, S. E. A review on the scientific understanding of heatwaves—their measurement, driving mechanisms, and changes at the global scale. *Atmos. Res.* **164–165**, 242–267 (2015).
37. Perkins, S. E. & Alexander, L. V. On the measurement of heat waves. *J. Clim.* **26**, 4500–4517 (2013).
38. Van Oldenborgh, G. J. et al. Cold waves are getting milder in the northern midlatitudes. *Environ.Res. Lett.* **14**, 114004 (2019).
39. van der Walt, A. J. & Fitchett, J. M. Trend analysis of cold extremes in South Africa: 1960–2016. *Int. J. Climatol.* **41**, 2060–2081 (2021).
40. Baldwin, J. W., Dessy, J. B., Vecchi, G. A. & Oppenheimer, M. Temporally compound heat wave events and global warming: an emerging hazard. *Earth's Future* **7**, 411–427 (2019).
41. Zscheischler, J. et al. A typology of compound weather and climate events. *Nat. Rev. Earth Environ.* **1**, 333–347 (2020).
42. Zscheischler, J. et al. Future climate risk from compound events. *Nat. Clim. Change* **8**, 469–477 (2018).
43. Ebi, K. L. & Bowen, K. Extreme events as sources of health vulnerability: drought as an example. *Weather Clim Extremes* **11**, 95–102 (2016).
44. Franken, O., Ferreira, S. S. D., Jesse, W. A. M., Berg, M. P. & Ellers, J. A common yardstick to measure the effects of different extreme climatic events on soil arthropod community composition using time-series data. *Front. Ecol. Evol.* **6**, https://doi.org/10.3389/fevo.2018.00195 (2018).
45. Ceccherini, G., Russo, S., Ameztoy, I., Romero, C. P. & Carmona-Moreno, C. Magnitude and frequency of heat and cold waves in recent decades: the case of South America. *Nat. Hazards Earth Syst. Sci.* **16**, 821–831 (2016).
46. Dosio, A., Mentaschi, L., Fischer, E. M. & Wyser, K. Extreme heat waves under 1.5 °C and 2 °C global warming. *Environ. Res. Lett.* **13**, 054006 (2018).
47. Nairn, J. R. & Fawcett, R. J. B. The excess heat factor: a metric for heatwave intensity and its use in classifying heatwave severity. *Int. J. Environ. Res. Public Health* **12**, 227–253 (2015).
48. de Perez, E. C. et al. Global predictability of temperature extremes. *Environ. Res. Lett.* **13**, 054017 (2018).
49. Cowan, T. et al. More frequent, longer, and hotter heat waves for Australia in the twenty-first century. *J. Clim.* **27**, 5851–5871 (2014).
50. Lovino, M. A., Müller, O. V., Berbery, E. H. & Müller, G. V. How have daily climate extremes changed in the recent past over northeastern Argentina? *Glob. Planetary Change* **168**, 78–97 (2018).
51. Herold, N., Ekström, M., Kala, J., Goldie, J. & Evans, J. Australian climate extremes in the 21st century according to a regional climate model ensemble: Implications for health and agriculture. *Weather Clim. Extremes* **20**, 54–68 (2018).
52. Orlowsky, B. & Seneviratne, S. I. Global changes in extreme events: regional and seasonal dimension. *Clim. Change* **110**, 669–696 (2012).
53. Perkins-Kirkpatrick, S. et al. Natural hazards in Australia: heatwaves. *Clim. Change* **139**, 101–114 (2016).
54. Perkins-Kirkpatrick, S. E. & Gibson, P. B. Changes in regional heatwave characteristics as a function of increasing global temperature. *Sci. Rep.* **7**, 12256 (2017).
55. Zhao, A., Bollasina, M. A. & Stevenson, D. S. Strong influence of aerosol reductions on future heatwaves. *Geophys.l Res. Lett.* **46**, 4913–4923 (2019).
56. Mascioli, N. R., Previdi, M., Fiore, A. M. & Ting, M. Timing and seasonality of the United States 'warming hole'. *Environ. Res. Lett.* **12**, 034008 (2017).
57. Partridge, T. F. et al. Spatially distinct seasonal patterns and forcings of the U.S. warming hole. *Geophys. Res. Lett.* **45**, 2055–2063 (2018).
58. Giorgi, F. & Lionello, P. Climate change projections for the Mediterranean region. *Glob. Planet. Change* **63**, 90–104 (2008).
59. Lelieveld, J. et al. Climate change and impacts in the Eastern Mediterranean and the Middle East. *Clim. Change* **114**, 667–687 (2012).
60. Diffenbaugh, N. S., Pal, J. S., Giorgi, F. & Gao, X. Heat stress intensification in the Mediterranean climate change hotspot. *Geophys. Res. Lett.* **34**, https://doi.org/10.1029/2007GL030000 (2007).
61. Lelieveld, J. et al. Strongly increasing heat extremes in the Middle East and North Africa (MENA) in the 21st century. *Clim. Change* **137**, 245–260 (2016).
62. Zittis, G. et al. Business-as-usual will lead to super and ultra-extreme heatwaves in the Middle East and North Africa. *npj Clim. Atmos. Sci.* **4**, 20 (2021).
63. Hulley, G. C., Dousset, B. & Kahn, B. H. Rising trends in heatwave metrics across Southern California. *Earth's Future* **8**, e2020EF001480 (2020).
64. Liu, W. et al. Spatiotemporal computing of cold wave characteristic in recent 52 years: a case study in Guangdong Province, South China. *Nat. Hazards* **79**, 1257–1274 (2015).
65. Spinoni, J. et al. Heat and cold waves trends in the Carpathian Region from 1961 to 2010. *Int. J. Clim.* **35**, 4197–4209 (2015).
66. Russo, S. et al. Magnitude of extreme heat waves in present climate and their projection in a warming world. *J. Geophys. Res.: Atmos.* **119**, 12,500–12,512 (2014).
67. Hersbach, H. et al. in *ERA5 Hourly Data on Single Levels from 1979 to Present* (2018).
68. Schoetter, R., Cattiaux, J. & Douville, H. Changes of western European heat wave characteristics projected by the CMIP5 ensemble. *Clim. Dynamics* **45**, 1601–1616 (2015).
69. Argüeso, D., Di Luca, A., Perkins-Kirkpatrick, S. E. & Evans, J. P. Seasonal mean temperature changes control future heat waves. *Geophys. Res. Lett.* **43**, 7653–7660 (2016).
70. Alghamdi, A. S. & Harrington, J. Trends and spatial pattern recognition of warm season hot temperatures in Saudi Arabia. *Theor. Appl. Climatol.* **138**, 793–807 (2019).
71. Geirinhas, J. L. et al. Characterizing the atmospheric conditions during the 2010 heatwave in Rio de Janeiro marked by excessive mortality rates. *Sci. Total Environ.* **650**, 796–808 (2019).
72. Ma, F. & Yuan, X. Impact of climate and population changes on the increasing exposure to summertime compound hot extremes. *Sci. Total Environ.* **772**, 145004 (2021).
73. Kunst, A. E., Looman, C. W. N. & Mackenbach, J. P. Outdoor air temperature and mortality in the Netherlands: a time-series analysis. *Am. J. Epidemiol.* **137**, 331–341 (1993).
74. Kendall, M. G. *Rank Correlation Methods* (1948).
75. Mann, H. B. Nonparametric tests against trend. *Econometrica: J. Econom. Soc.* **13**, 245–259 (1945).
76. Hamed, K. H. & Rao, A. R. A modified Mann-Kendall trend test for autocorrelated data. *J. Hydrol.* **204**, 182–196 (1998).
77. Sen, P. K. Estimates of the regression coefficient based on Kendall's tau. *J. Am. Stat. Assoc.* **63**, 1379–1389 (1968).

Acknowledgements

This research is supported by the Strategic Priority Research Program of Chinese Academy of Sciences (grant no. XDA 20030302) and the Southern Marine Science and Engineering Guangdong Laboratory (Zhuhai) (grant no. 311020017).

Author contributions

Y.Z., Q.L. and Y.G. designed research; Y.Z., X.D. and H.W. downloaded and processed ERA5 data; Y.Z. conducted the analysis; Y.Z. and Q.L. wrote the manuscript. All the authors contributed to manuscript editing.

Competing interests

The authors declare no competing interests.

Additional information

Supplementary information The online version contains supplementary material available at https://doi.org/10.1038/s43247-022-00404-x.

Correspondence and requests for materials should be addressed to Qiangzi Li or Yong Ge.

Peer review information *Communications Earth & Environment* thanks Adriaan van der Walt and the other, anonymous, reviewer(s) for their contribution to the peer review of this work. Primary Handling Editor: Heike Langenberg.